

# International Conference on Space Optics—ICSO 2018

Chania, Greece

9–12 October 2018

*Edited by Zoran Sodnik, Nikos Karafolas, and Bruno Cugny*



## *Design and on-orbit calibration of the solar ultraviolet imager (SUVI) on the GOES-R series weather satellite*

*Gopal Vasudevan*

*Lawrence Shing*

*Dnyanesh Mathur*

*Christopher Edwards*

*et al.*



# Design and On-Orbit Calibration of the Solar UltraViolet Imager (SUVI) on the GOES-R Series Weather Satellite

Gopal Vasudevan<sup>1</sup>, Lawrence Shing<sup>1</sup>, Dnyanesh Mathur<sup>1</sup>, Christopher Edwards<sup>1</sup>, Margaret Shaw<sup>1</sup>, Daniel Seaton<sup>2,3</sup>, Jonathan Darnel<sup>2,3</sup>

<sup>1</sup>Lockheed Martin Advanced Technology Center, 3251 Hanover Dr., Palo Alto, CA 94304

<sup>2</sup>NOAA/National Centers for Environmental Information, 325 Broadway, Boulder CO 80305

<sup>3</sup>University of Colorado, 216 UCB, University of Colorado Boulder Campus, Boulder, CO 80309

## ABSTRACT

The GOES-R series is the latest in a long line of American geostationary weather satellites operated by NOAA (National Oceanic and Atmospheric Administration). The Solar Ultraviolet Imager (SUVI) is an instrument onboard Geostationary Operational Environmental Satellites, GOES-R series, part of NOAA's (National Oceanic and Atmospheric Administration) space weather monitoring fleet. GOES-16 SUVI is in operation and the GOES-17 SUVI has completed initial calibrations.

SUVI is a generalized Cassegrain telescope with a large field of view that employs multilayer coatings optimized to operate in six extreme ultraviolet (EUV) narrow bandpasses centered at 9.4, 13.1, 17.1, 19.5, 28.4 and 30.4 nm. The SUVI EUV line set provides the best comprehensive feature and dynamics information for revealing and correlating both the low coronal signatures of coronal mass ejections (CME) triggers (for example, flares) and the high coronal signatures of the actual CME. SUVI acquires full disk images in EUV band pass every few minutes and telemeters the data to the ground for digital processing. These data will enable NOAA to monitor solar activity and to issue accurate near real-time alerts when space weather may possibly affect the performance and reliability of space-borne and ground-based technological systems and human endeavors.

This paper describes key design drivers in the development of SUVI, methods used in the autonomous on-orbit calibration of the instrument, and the automated monitoring of the health and safety of the instrument during operations.

**Keywords:** Extreme ultraviolet, Imager, Calibration

## 1 INTRODUCTION

The Solar Ultraviolet Imager on the GOES-16 spacecraft, launched November 19, 2016, and on the GOES-17 spacecraft, launched on March 1, 2018, are two in a line of four instruments of the same design that will image the Sun's atmosphere in the extreme ultraviolet waveband for the next 20 years.

The SUVI operational goals are to: locate coronal holes for geomagnetic storm forecasts, detect and locate flares for forecasts of solar energetic particle events related to flares, monitor changes in the corona that indicate coronal mass ejections (CMEs) detect active regions beyond the east limb for space weather forecasts, and analyze active region complexity for flare forecasts.

Table 1: SUVI Bandpass Channels and their Associated Solar Phenomena

Passband	Spectral Lines	Temp. (K)	Observed Phenomena
9.4nm	Fe X	$1.1 \times 10^6$	Active Regions
	Fe XVII	$7.1 \times 10^6$	Solar Flares
13.1nm	Fe VII	$4.0 \times 10^5$	Quiet Sun
	Fe XXI	$1.1 \times 10^7$	Solar Flares
17.1nm	Fe IX	$7.0 \times 10^5$	Transition Region
	Fe X	$1.1 \times 10^6$	Corona
19.5nm	Fe XI	$1.4 \times 10^6$	Active Regions and
	Fe XII	$1.6 \times 10^6$	Coronal holes
	Fe XXIV	$1.8 \times 10^7$	Strong Solar Flares
28.4nm	Fe XV	$2.2 \times 10^6$	Active Regions
30.4nm	He II	$5.0 \times 10^4$	Chromosphere, Prominences
	Si IX	$1.6 \times 10^6$	Active Regions

SUVI's six passbands — centered at 9.4, 13.1, 17.1, 19.5, 28.4 and 30.4 nm — provide images of the solar chromosphere and corona over a temperature range from about 50,000 K to 10 million K. The measurements enable tracking phenomena such as solar prominences, coronal holes, active regions, and dynamic events such as solar eruptions and flares. SUVI is distinguished among other EUV solar imagers by its relatively large field of view, which enables the study of the process of magnetic reconnection that powers solar flares.

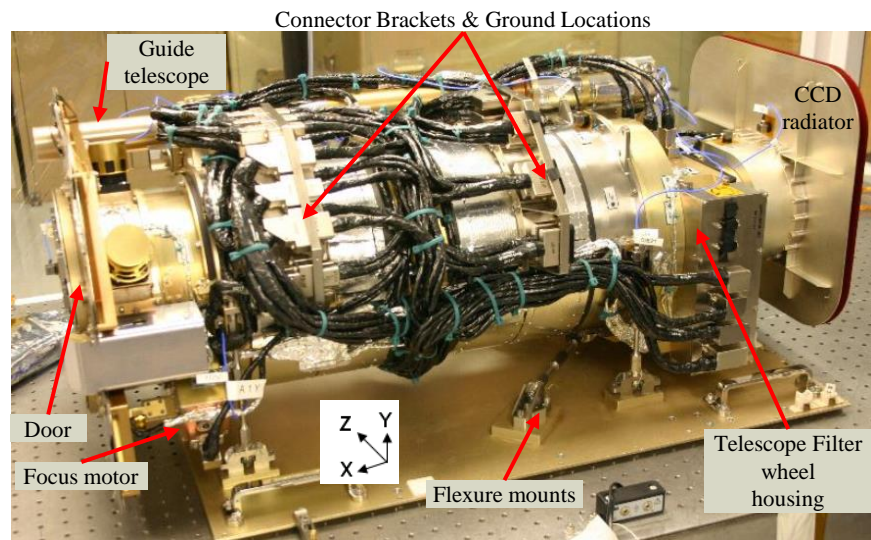


Figure 1: SUVI Telescope overview

SUVI is a generalized Cassegrain telescope (Figure 1) with a 20cm physical diameter primary mirror and a 9cm diameter secondary mirror (Ref. [1] [2]). Both the primary and secondary mirrors have multilayer coatings that define six wavelength bands (9.4, 13.1, 17.1, 19.5, 28.4 and 30.4 nm) spanning the extreme ultraviolet (EUV) spectrum (Figure 2). An aperture selector is used to illuminate the appropriate channel.

In order to attenuate the off-band light, a set of thin film filters are placed in the optical path ahead of the primary mirror. SUVI nominally uses 200 nm thick Zirconium in front of the 9.4nm and 13.1 nm channels, and 150 nm thick Aluminum in front of the remaining channels. Further attenuation is achieved by placing thin films near the focal plane on a filter wheel.

SUVI uses a Teledyne-E2V provided back-illuminated thinned passively cooled CCD to collect the Solar images. The imaging region uses 1280x1280 pixels to image a 53.3 arcmin x 53.3 arcmin field.

The SUVI telescope resides on a sun-pointing platform on the Solar array. The sun-pointing platform is controlled to maintain sun pointing to better than 1arcsec using the error signals from a high data rate guide telescope.

The SUVI instruments are designed to provide effective operational Solar patrol service with an expected mission lifetime of 20+ years. The SUVI flight software provides a flexible image sequencing capability for long-term solar monitoring. It is designed to control instrument sub-systems (heaters, mechanisms, camera and guide telescope) as well as managing the communications with the spacecraft, during all phases of the mission. The flight software is comprised of four items with specific functionality – startup read-only memory code, SpaceWire ASIC ROM code, Kernel, and the flight software application. The primary responsibility of startup ROM code is to boot up the RAD750 processor into a deterministic state. The SpaceWire ASIC ROM code provides data routing between the spacecraft, RAD750 processor, and the camera. The Kernel provides task scheduler, file system and also includes the capability of running on-board scripts. The flight software application (FSA) component provides the control of the instrument sub-systems to enable image acquisition, thermal control, analog data acquisition (temperatures, voltages, currents), and computation of error signals from guide telescope to meet all mission requirements. The FSA also includes fault detection and limit monitoring capabilities. The software is

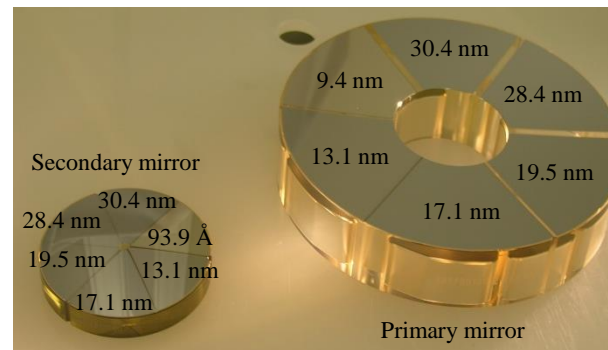


Figure 2: Multilayer mirror coatings provide appropriate bandpasses.

designed to operate autonomously to acquire not only patrol images but also most of the calibration data as described in the next section.

## 2 ON-ORBIT SUVI CHARACTERIZATION AND CALIBRATION

Regular calibrations are essential and critical for proper operations of an instrument during long-term missions. The calibrations include re-characterizations over the mission durations of the camera gain, camera flat-fields and vignetting corrections, dark images, and filter transmissivities. However, manual calibrations impose an often-unavoidable demand on ground operations personnel. A sequencer and script system software are built into the instrument control software to enable minimal operator load and minimal disruption to science data acquisition. Thus, data is automatically taken for camera gain, dark images, filter transmissivities, allowing these quantities to be characterized and updated periodically over the life of the mission. In contrast, flat-field data acquisition requires operator scheduling because it involves coordination with the spacecraft. The approach for flat-field calibration uses a scanning approach (a boustrophedon maneuver), which takes smeared images (Ref. [3]).

The SUVI Sequencer is designed to take images at a regular cadence. The image to be acquired is chosen from a list of prioritized image lists. While a sequence is running, the highest priority image scheduled at each time slot is selected and taken. In order to meet certain operational requirements, a four-minute sequence was generated that runs continuously unless interrupted by some event. The four-minute sequence is comprised of 24 ten-second slots (Figure 3). Two slots are primarily dedicated for calibration activities. When not used for calibration, the two slots are used for additional science images.

Minute	1						2						3						4					
Image No	1	2	3	4	5	6	7	8	9	10	11	12	13	14	15	16	17	18	19	20	21	22	23	24
Exp Time [ms]	1000	5	5	1000	5	-	-	1000	5	5	1000	5	1000	5	5	1000	5	1000	1000	5	1000	5	1000	5
Time	0:10	0:20	0:30	0:40	0:50	1:00	1:10	1:20	1:30	1:40	1:50	2:00	2:10	2:20	2:30	2:40	2:50	3:00	3:10	3:20	3:30	3:40	3:50	4:00
Channel	9.4nm	9.4nm	9.4nm	19.5nm	19.5nm	Cal	Cal	13.1nm	13.1nm	13.1nm	19.5nm	19.5nm	9.4nm	9.4nm	9.4nm	17.1nm	17.1nm	19.5nm	28.4nm	28.4nm	30.4nm	30.4nm	19.5nm	19.5nm
Eclipse Flag	Eclipse Scripts to acquire data for mechanisms																							

Figure 3: SUVI’s nominal observing sequence acquires complete passband and dynamic range images at least once every four minutes

By selecting a set of sequences and staggering the cadences of the sequences, a large fraction of regular on-board calibration activities is automated, allowing SUVI to be operated with little manual commanding from the ground and little interruption to nominal science data sequencing. For example, the calibration slots are used for taking dark images, images for monitoring the health of the entrance and focal plane filters, and images at various exposure durations used to calculate the light transfer curves and obtain camera gains. The calibration slots are also used to run brief mechanism setting checks.

A script is a sequential list of statements which can include commands to issue to SUVI and conditional statements to test telemetry values along with branching to other line numbers, assertions, timed delays and conditional waits. SUVI scripts can send any command in the command database. A script is first loaded into one of 16 slots and then run by an automated command (e.g., from the sequencer), a spacecraft script, or a manual command from the operator. Typically, scripts are started by conditional events such as eclipses or temperature limit violations, or they are scheduled into the nominal sequence in the calibration slot.

Some calibrations require longer time periods than are available during the calibration slots in a normal sequence. These calibrations include dark current characterizations and mechanism characterizations. An approach used by SUVI is to use eclipse periods for these calibrations. Eclipse seasons occur twice a year with periods of up to 67 minutes of non-observing

time. The eclipse seasons lasts approximately 42 consecutive days. Six of the longest eclipse time periods are used for performing long duration calibrations.

During an eclipse period, an automated set of commands are run by the spacecraft that lets SUVI know that the spacecraft has entered the umbra of an eclipse. SUVI on-board scripts decide whether the particular eclipse is in the middle of eclipse season (eclipses in the middle of eclipse season will last ~60+ minutes). If so, a set of automated chained scripts run the mechanism characterization or the dark current characterization tests based on the eclipse day. At the end of the scripted test, the software automatically reverts to operational sequencing.

### 2.1 Camera-CCD System Characterization

The SUVI aliveness check LED can also be used to characterize the system gain. The illumination of the focal plane by the LED is non-uniform. We take advantage of the non-uniform illumination to obtain image pairs with a range of signal levels. These Light Transfer Curve (LTC) images using the LED were taken in ground tests, and during Post Launch Testing (PLT).

The LED is not expected to remain usable for the entire duration of the mission. Therefore, other means of obtaining LTC images using diffuse scattered light will be used to trend the system gain throughout the mission.

### 2.2 Dark Current

The focal plane temperature can be regulated by operational heaters. The SUVI focal plane has its own radiator as shown in figure 1. The radiator's efficiency can be affected by seasonal and diurnal affects. To maintain a steady temperature throughout the year, a setpoint that maintains closed loop control is chosen. i.e. the CCD temperature is not allowed to drift to a temperature defined by the radiator.

During PLT, we used the operational heaters to achieve temperature setpoints to obtain the dark current profile of the CCD at BOL. Figure 5 shows the dark current vs temperature for the PLT data. As expected, the CCD's dark current at BOL agrees with ground test data. The dark current is expected to increase over the duration of the mission due to radiation environments.

### 2.3 Flat-Field

As described in (Ref. [3]), the flatfield response of the SUVI focal plane is measured on-orbit for each of the SUVI channels. The boustrophedon method of smearing the solar image across the focal plane relies on the smooth motion of the Solar Pointing Platform (SPP) on which SUVI is mounted. Several scans are required for each filter combination in order to measure the response across the entire focal plane.

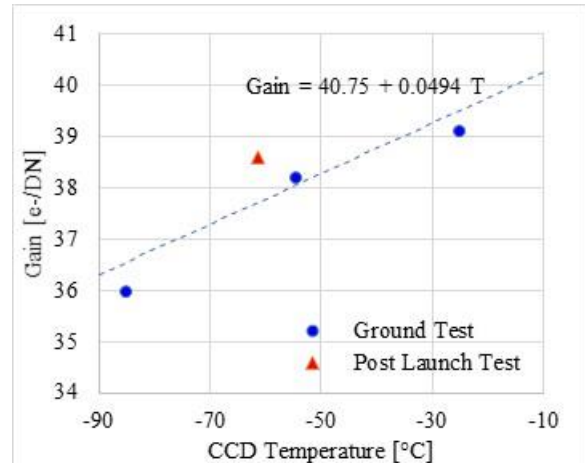


Figure 4: Gain vs Temperature fit using ground test data and corroborating PLT data

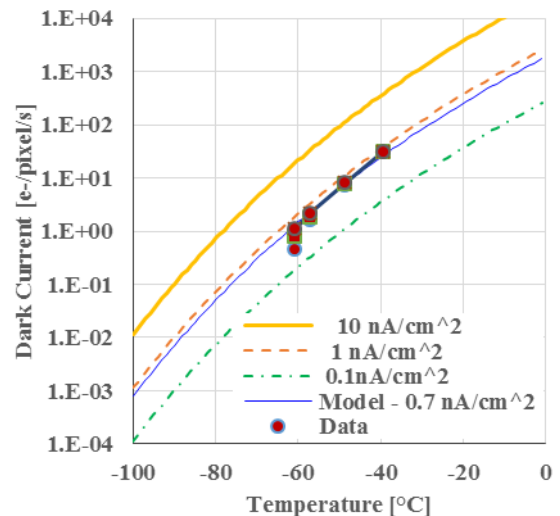


Figure 5: Dark current variation over temperature matched ground test results

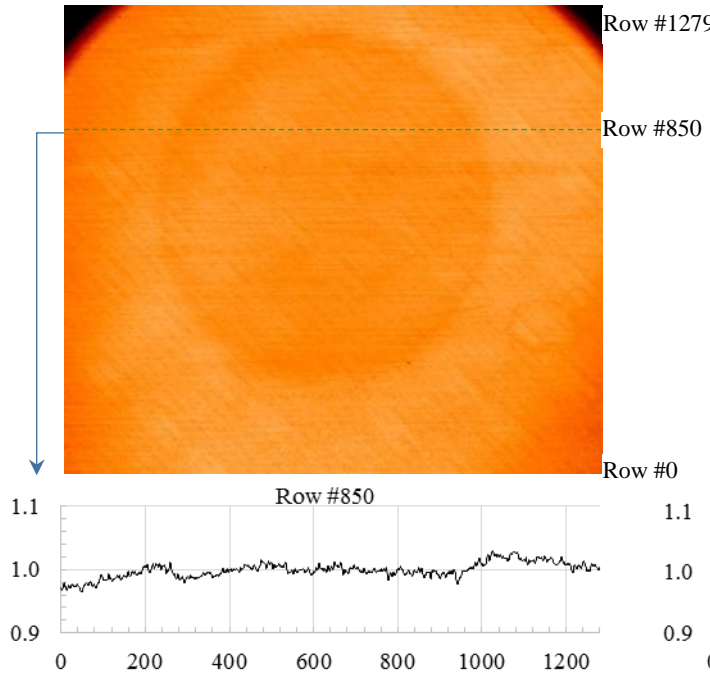


Figure 6a. SUVI GOES-16 30.4nm flatfield ~1 year into mission.

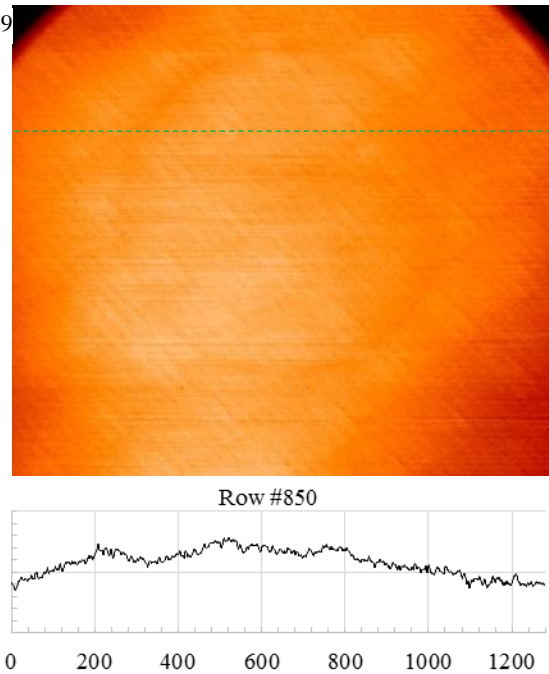


Figure 6b. SUVI GOES-17 30.4nm flatfield ~2 months into mission.

Using the same optical paths and filters as SUVI’s observing sequence, we can quite efficiently generate the flatfield response for each channel. This in-situ measurement by default folds in the solar spectrum with the spectral response of the analysis filters and multilayer mirror reflectivity onto the back illuminated CCD at the focal plane.

Figures 6a and 6b show the normalized response of the SUVI focal planes in GOES-16 and GOES-17 using the Thin Al/Open filter combination. The vignetting in the upper left and right are expected; other channels will have vignetting in different corners. The circular dip in response is coincident with the constant position of the solar disk on the focal plane; the dip in figure 6a is ~2%. The diminished response is expected over the course of the mission due to EUV exposure of the focal plane. The large-scale diagonal striations that appear are intrinsic to the CCD’s response to 30.4nm. Some horizontal features are residual artifacts from the processing of the boustrophedon scans.

#### 2.4 Focal plane filter transmissivities

In lieu of using ground test data, or modeling of thin film transmission of the analysis filters, SUVI image data can be used to determine the absolute filter transmission of the thin filters in the two independent filter wheels.

The boustrophedon dataset has images that have permutations of the two thin analysis filters. For the 17.1, 19.5, 28.4 and 30.4 nm channels this involves collecting data with the 3 out of 4 permutations of the Thin Al and Open filter positions; note, Open/Open is not usable for filter characterization as there will be white light contamination in the images. We rely on the solar output staying constant over the ~30 minute timescale of the dataset for each channel. Excluding sections that contain active regions reduces the variability in the results. For the case of the 9.4 and 13.1 nm channels, the filters permuted are Thin Zr and

Table 2: Filter transmission of individual analysis filters in SUVI on GOES-17

Wavelength (nm)	Filter	Location	Transmission	
			Model	Measured
9.4	Thin Zr	Filter 1	0.366	0.359
		Filter 2	0.366	0.345
13.1	Thin Zr	Filter 1	0.328	0.306
		Filter 2	0.328	0.297
17.1	Thin Al	Filter 1	0.539	0.500
		Filter 2	0.536	0.483
19.5	Thin Al	Filter 1	0.533	0.490
		Filter 2	0.531	0.474
28.4	Thin Al	Filter 1	0.390	0.347
		Filter 2	0.387	0.320
30.4	Thin Al	Filter 1	0.368	0.335
		Filter 2	0.366	0.308

Open filter positions. Table 2. shows the on-orbit measured filter transmissions of the respective channels. The modeled transmission is estimated given filter thickness, oxide layer, residual epoxy, and mesh properties.

Due to the weak signal in the 9.4nm channel, its boustrophedon data could not be used for the filter transmission measurements. Special calibration images using binned images with the required filter permutations were used for the 9.4nm filter transmission measurements.

Although filter transmission can be measured in all the channels using similar binned images and filter permutations, the existing boustrophedon dataset was used to extract the same data.

Prior to measuring on-orbit filter transmissivities, we relied on the modeled values for the filters in our metrology. The measured throughput more closely represents the filter characteristics and can be trended over the course of the mission.

### 2.5 Focus Mechanism

The SUVI instrument has a focus mechanism that can adjust the position of the secondary mirror. A set of images at each wave band is taken at various focus positions. These focus sweeps are taken one wavelength at a time in order to minimize any variation due to evolution of the solar image affecting the data analysis

28 regions of interest (ROI) were analyzed at each waveband. The ROIs ranged from the center of the solar disk to areas including the limb. Figure 7 shows the approximate position of the ROIs in the 1280x1280 SUVI focal plane. The circular outline is the position of the solar limb.

The FFT of the ROIs were used to measure the relative power in the high frequency components in each ROI. This is used as the indicator of the contrast of the solar features in the images as we sweep through different focus positions. Figure 8 shows the normalized contrast plots of the 12 mid-radii locations (indicated in blue letters in Figure 7); each color in Figure 8 is a different ROI on the disk. Note, the contrast does not change appreciably within 10 steps of best focus.

Table 3 summarizes the focus data taken on 5/30/2018 for SUVI on GOES-17. From these results we chose a single focus position of 45 to use at BOL. Focus sweeps will be collected on a bi-annual basis to obtain focus positions and determine if focus adjustments are needed.

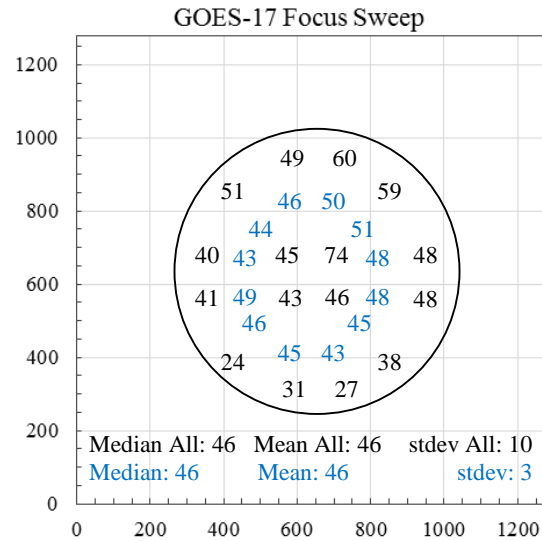


Figure 7: SUVI GOES-17 best focus mosaic for 17.1nm. Each number in the disk indicates the best focus fit for that ROI location from the 17.1nm focus sweep dataset.

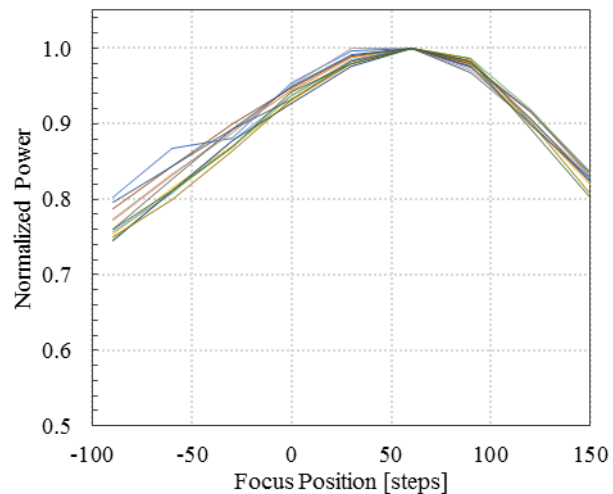


Figure 8: Normalized power vs focus position plot of SUVI GOES-17 17.1nm focus sweep.

## 2.6 CCD Plate Scale

In ground tests, the plate scale of the SUVI instrument was measured optically with visible light. The precise movement of a test target was imaged, and the derived plate scale was determined to be 2.50 arcseconds/pixel. Due to launch conditions, or the EUV optical behavior differing from the optical ground tests, or even different focus positions, the plate scale can change.

On-orbit, we can remeasure the plate scale by measuring the diameter of the solar images and cross-calibrating the instrument with other solar observatories. At Lockheed Martin, we have developed routines to measure the diameters, and radial centers of solar images. [Ref. [4]] Measuring the diameter of the sun in EUV is not a simple task as the limb is not a well-defined feature. For this reason, we generally discard the 30.4nm limb fit image analysis.

After the best focus is set as described in Section 2.4, numerous images can be compared to similar images from other observatories, whose plate scales have already been determined. The AIA instrument provided the reference for this cross-calibration. AIA's plate scale was measured precisely on orbit using image data from the Venus transit in 2012.

Using the same limbfit routines on the AIA data and SUVI data from GOES-16, SUVI's plate scale was determined to be 2.506 arcseconds/pixel. Using SUVI GOES-16 as the new reference, SUVI GOES-17 was cross-calibrated and its plate scale is expected to be 2.501 arcseconds/pixel. The on-orbit plate scale concurs with the ground test measurements.

## 2.7 Effective Area

The output of SUVI is an image of digital number (DN) values corresponding to the spectral radiance integrated over the solid angle of each pixel and the passband of the specific channel. The throughput efficiency of the specific channel is thus given by the product of the reflectivities of the primary and secondary mirrors (Ref. [2]), the specific entrance filter transmissivity, the filter wheel filter transmissivities, and the effective quantum efficiency (Ref [5]).

The filter transmissivities are obtained using optical constants taken from Lawrence Livermore National Labs CXRO database ([6]). There is some uncertainty in applying the model especially for the Aluminum thin filters due to the rapidly varying optical constants near the Aluminum L<sub>2,3</sub> absorption edge (close to 17.0 nm). The filter transmissivities were determined by using the measured thin film thickness, and estimating the thicknesses of the oxide layers and epoxy layers by fitting a model to measured transmittances of some filter coupons. The models were re-adjusted based on fitting the on-orbit measurements and constraining the thicknesses of the thin-films.

In general, some amount of contamination layer builds up over time. Typically, the contamination layers are molecular hydrocarbons that stem from effluence from different spacecraft and instrument subsystems. The contamination layers degrade the throughput performance. The effective area is obtained by multiplying the geometric area with the throughput efficiency:

$$A_{eff}(\lambda) = A_i PM(\lambda) SM(\lambda) Ent(\lambda) FW1(\lambda) FW2(\lambda) EQE(\lambda) D(\lambda), \quad [1]$$

where,  $D(\lambda)$ , is the throughput loss due to contamination build up or any other degrading factor.

Since it is very difficult to obtain a well-calibrated, narrow band, and collimated EUV source, a full spectral calibration of the effective area is not feasible. Instead, component-level measurements are used to produce the effective areas. This approach has been used in the calibrations of TRACE (Ref. [7]), EIT (Ref. [8]), and AIA (Ref. [9]).

The effective areas, without the contamination layer degradation, of the six channels for GOES-16 and GOES-17 SUVI flight models are shown in Figure 9.

Table 3: Best focus positions for SUVI GOES-17 at each channel.

Wavelength (nm)	Median	stdev
9.4	37.8	11.6
131	43.1	6.1
17.1	46.9	2.7
19.5	45.5	5.8
28.4	41.4	3.4
30.4	55.9	4.1
median	44.3	
mean	45.1	
stdev	6.2	

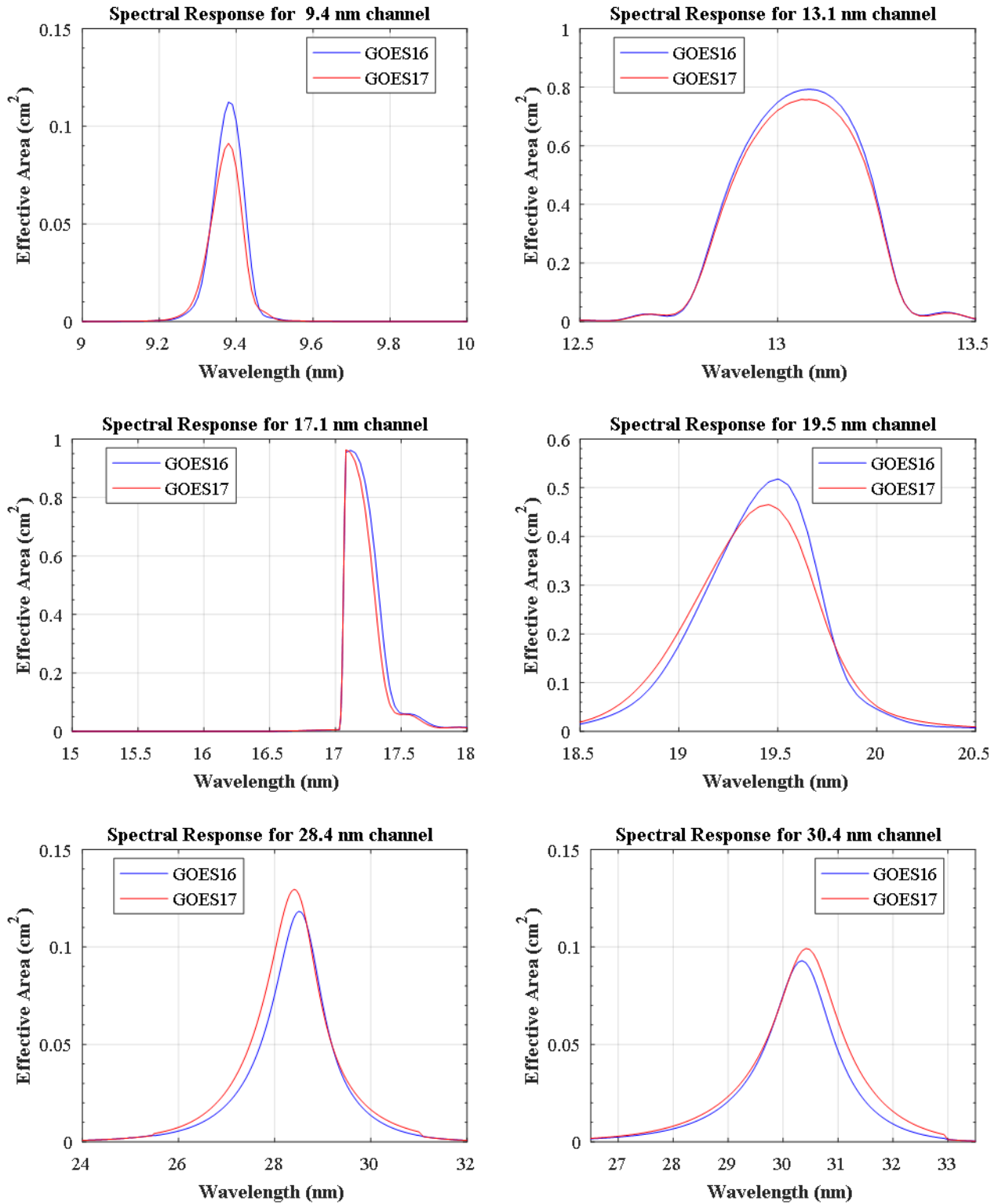


Figure 9: Effective areas for GOES-16 and GOES-17 SUVI are very similar in response.

### 3 CONCLUSIONS

Enabled by the SUVI flight software and sequencer architecture, the automated system to characterize and calibrate SUVI allows SUVI to be operated with little manual commanding from the ground and little interruption to nominal sequencing. The automated data acquisition system also would lend itself to automated trending and monitoring tools to further reduce operator and analyst burden throughout the instrument lifetime.

Two flight instruments have been characterized and calibrated and are currently undergoing validation testing. GOES-16 has now been on orbit for about 18 months and GOES-17 for about 5 months at the time of paper submission. Both instruments are operating within operational parameters. At the end of validation testing, SUVI will provide contextual images for space weather forecasting for next two decades.

### 4 REFERENCES

- [1] D. Martínez-Galarce, J. Harvey, M. Bruner, J. Lemen, E. Gullikson, R. Soufli, E. Prast and S. Khatri, "A novel forward-model technique for estimating EUV imaging performance - design and analysis of the SUVI telescope," in *Proc. SPIE Vol. 7732, Space Telescopes and Instrumentation 2010: Ultraviolet to Gamma Ray*, San Diego, CA, 2010.
- [2] D. Martínez-Galarce, R. Soufli, D. Windt, M. Bruner, E. Gullikson, S. Khatri, E. Spiller, J. Robinson, S. Baker and E. Prast, "Multisegmented, multilayer-coated mirrors for the Solar Ultraviolet Imager," *Optical Engineering*, vol. 52, no. 9, 2013.
- [3] L. Shing, C. Edwards, D. Mathur, G. Vasudevan, M. Shaw and C. Nwachuku, "GOES-R SUVI EUV Flatfields Generated Using Boustrophedon Scans," in *American Geophysical Union, Fall Meeting 2017*, New Orleans, LA, 2017.
- [4] S. Freeland and B. Handy, "Data Analysis with the SolarSoft System," *Solar Physics*, vol. 182, no. 2, pp. 497-500, 1998.
- [5] R. Stern, L. Shing and M. Bloucke, "Quantum efficiency measurements and modeling of ion-implanted, laser-annealed charge-coupled devices: x-ray, extreme-ultraviolet, ultraviolet, and optical data," *Applied Optics*, vol. 33, no. 13, pp. 2521-2533, 1994.
- [6] B. Henke, E. Gullikson and J. Davis, "X-Ray Interactions: Photoabsorption, Scattering, Transmission, and Reflection at  $E = 50\text{-}30,000$  eV,  $Z = 1\text{-}92$ ," *Atomic Data and Nuclear Data Tables*, vol. 54, no. 2, pp. 181-342, 1993.
- [7] B. Handy, L. Acton, C. Kankelborg, C. Wolfson, D. Akin, M. Bruner, R. Carvalho, R. Catura, R. Chevalier, D. Duncan, C. Edwards, C. Feinstein, S. Freeland, F. Friedlaender, C. Hoffmann, N. Hurlburt and B. Jurcevich, "The transition region and coronal explorer," *Solar Physics*, vol. 187, no. 2, pp. 229-260, 1999.
- [8] K. Dere, J. Moses, J.-P. Delaboudinière, J. Brunaud, C. Carabetian, J.-F. Hochedez, X. Song, R. Catura, F. Clette and J.-M. Defise, "The Preflight Photometric Calibration of the Extreme-Ultraviolet Imaging Telescope EIT," *Solar Physics*, vol. 195, no. 1, pp. 13-44, 2000.
- [9] P. Boerner, C. Edwards, J. Lemen, A. Rausch, C. Schrijver, R. Shine, L. Shing, R. Stern, T. Tarbell, A. Title, C. Wolfson, R. Soufli, E. Spiller, E. Gullikson, D. McKenzie and D. Windt, "Initial Calibration of the Atmospheric Imaging Assembly (AIA) on the Solar Dynamics Observatory (SDO)," *Solar Physics*, vol. 275, no. 1-2, pp. 41-66, 2012.